The 1st Joint International Conference on Multibody System Dynamics
May 25-27, 2010, Lappeenranta, Finland

A Dynamic Model of an Overhung Rotor with Deep-Groove Ball Bearings

Onur Cakmak*, Kenan Y. Sanliturk*

* Istanbul Technical University
Faculty of Mechanical Engineering
Vibration and Acoustics Laboratory
Inonu Cad. No: 87 Gumussuyu, 34437, Istanbul, Turkey
email:cakmakon@yahoo.com, sanliturk@itu.edu.tr

ABSTRACT

A ball bearing consisting of rolling elements, inner and outer rings and a cage structure can be described as a multi-body system. In order to predict the dynamic behavior and resonance characteristics of a rotor-ball bearing system, it can be modelled and analysed as a multi-body system with flexible and rigid parts. In this paper, a ball bearing is modelled with multi-body system approach by using Msc. ADAMS commercial software. The Hertzian theory is used for modelling the contact dynamics between the balls and rings. The ball bearing model is then assembled with the rotor model which comprised a shaft and a disc positioned at the free end of the shaft. For the flexible shaft case, the Multi-body system (MBS) model also included a Finite Element (FE) model of the shaft. The ball bearing model is used with both flexible and rigid shaft assumptions in order to highlight the differences between the two cases. As expected, it is necessary to include the flexibility of the shaft in the model, in order to to predict the changes in the modal characteristics of the system as a function of the rotor speed. Furthermore, including the gyroscopic effects leads to observe the forward and backward travelling modes with different natural frequencies.

The effects of the bearing diametral clearance and localized defects on the inner and outer rings are modelled and analysed using the model developed. Also, the effects of the rotor unbalance on the vibration level of the whole system are examined. A test rig – consisting of two ball bearings, a shaft and a disk - is also designed and developed so as to validate the theoretical model using experimental data. Order tracking and modal analyses were carried out and Campbell diagrams were obtained. Finally, the theoretical and the experimental results are compared and a refined MBS model is obtained for further analyses.

Keywords: ball bearings, vibrations, dynamic analysis, MBS model, gyroscopic effects.

1 INTRODUCTION

Understanding the vibration generated and transmitted through ball bearings is a significant task when the global vibrations of a rotating machinery are to be modelled and analysed. The studies about ball bearing vibrations are generally focused on the issues of predictive maintenance, fault diagnostics and condition monitoring which are mostly interested in detecting the defective bearings. However, when bearings are coupled with other structural components of a rotating machinery, bearings without any defect can also cause excessive vibrations due to the resonance characteristics.

In most of the published literature, the effects of various defects on vibration characteristics of ball bearings are studied [1, 2]. The defects that cause excessive vibrations can be localized or distributed on the rings or rolling elements of a ball bearing. Important clues about fault diagnosis of a rotating machinery can be obtained via observing the bearing-induced vibrations. Tandon and Choudry [1] in 1997 studied the vibration response of rolling element bearings with localized defects on their rings using analytical approach. They assumed that the bearing rings are isolated continuous systems and then obtained the equations of motion by using Lagrange's equations. The effects of the localized defects are assumed as pulses which are implemented as generalized forces in the Lagrange's equations. The vibration response of rolling bearings due to distributed defects is also studied by Tandon et al. [2]. First, they obtained the vibration response of a bearing without any defect. Then, a Fourier series expansion is used in order to determine the vibration amplitude at cage frequency and its

harmonics. The comparison between the defected and ideal models showed that for the defected case, outer and inner races have a response having a spectrum with peaks at characteristic defect frequencies for respective races.

Some of the specific features of ball bearings can also have significant effects on the dynamic behaviour and vibration characteristics of the system. Radial clearance, number of balls and preload are these features whose effects on vibrations are studied by several authors [3-6]. Tiwari et al. [3] had a study about the effect of radial clearance to vibration response of a balanced rotor. The differential equations were obtained with an assumption of linearized stiffness [4]. They also improved their model for the unbalanced rotor case [5]. A study about the effects of balls and preload on vibrations of bearings is carried out by Akturk et al. [6]. For a system with no defects, a theoretical investigation was made in order to determine whether the amount of preload and the change in number of balls could reduce the effects of ball-passing vibrations. The stiffness of the ball bearing was determined using the Hertzian contact approach and the damping generated from the elastohydrodynamic film or from any friction at various contacts was neglected. Researchers also developed numerical models for rotor-ball bearing systems. Wensing [7] built a deep groove ball bearing model by using Component Mode Synthesis (CMS) method. Finite Element (FE) models of individual components of a ball bearing, shaft and housings are built, then a model reduction is carried out in order to reduce the computation time. That study also contains the experimental validation of the model proposed. Sopanen and Mikkola [8, 9] developed a numerical ball bearing model which was integrated into a model of an electric motor. In that study, the model was found to be capable of representing the misalignments, waviness of the rings and their significant effects. Experimental studies of ball bearings are also very common and some of them are directed towards validating numerical models [7], [10].

This paper presents a dynamic model of an overhung rotor-ball bearing system. The model is built using Msc. ADAMS commercial software. First, a ball bearing model is introduced. Then, the rotor comprising a disc at the end of the shaft is assembled. Both rigid and flexible shaft models are used during the simulations. The flexible shaft is modelled using FE approach with beam elements. A numerical modal analysis is performed and natural frequencies are obtained for the flexible shaft case. Gyroscopic effects are also included and speed dependent natural frequencies are obtained. A run-up procedure is carried out and Campbell diagrams are obtained in order to observe the rotation speed dependent vibrations and critical speeds. The analyses are repeated with differing diametral clearance, unbalance and defect conditions. A test rig is designed with an overhung rotor supported by two ball bearings in order to use for validation purposes. Experimental modal analysis and order tracking analysis techniques are utilised during this process.

The outline of this paper is as follows. First, a theoretical background about ball bearing dynamics is introduced. The analytical procedure of calculating contact stiffness between ball bearing components are summarised. Also, the kinematics of a ball bearing and defect frequencies are briefly described. The steps of MBS modelling process of the rotor-ball bearing system are introduced. After that the test rig design and the measurement procedures are described. Then, comparisons of the numerical and experimental results are presented in terms of natural frequencies and amplitude spectrums. Finally, some concluding remarks are given.

2 THEORY

2.1 Contact Stiffness at Ball Bearings

Loads acting between rolling elements and raceways develop only small contact areas [11]. Stiffness at these contacts is calculated by using Hertzian Theory. If the ball bearings are running at high operational speeds, lubrication must be taken into account when modelling their dynamics [8]. This type of contact is called elastohydrodynamic (EHL) contacts. The stiffness and damping effects of the lubrication film is neglected in this study.

The rolling elements in a ball bearing are in contact with the inner and outer raceway [7]. Figure 1 shows major geometric features of these contacting bodies and ball bearing:

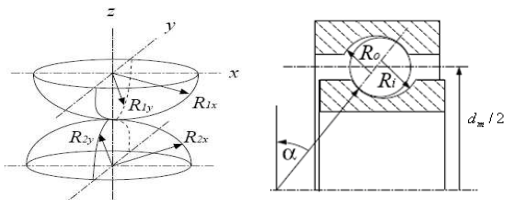

a) b)

Figure 1. a) Contacting bodies b) Geometric features of the contact region of a ball bearing [7]

If R_{re} represents the radius of the ball itself, the radiuses of the curvatures for the inner contact are:

$$R_{1x} = R_{re} \tag{1}$$

$$R_{1y} = R_{re} \tag{2}$$

$$R_{2x} = \frac{d_m / 2}{\cos(\alpha)} - R_{re} \tag{3}$$

$$R_{2y} = -R_i \tag{4}$$

In a similar manner, the radii of curvature for the outer contacts are:

$$R_{2x} = -(\frac{d_m / 2}{\cos(\alpha)} + R_{re}) \tag{5}$$

$$R_{2y} = -R_o \tag{6}$$

When calculating the curvature radiuses of the contacting surfaces, the assumption of a zero degrees contact angle (α) can give satisfactory results for deep-groove ball bearings[7]. The geometric features between two contacting solids can be expressed in terms of the curvature sum R, and curvature difference R_d, which are described in [7] as

$$\frac{1}{R} = \frac{1}{R_x} + \frac{1}{R_y} \tag{7}$$

$$R_d = R(\frac{1}{R_x} - \frac{1}{R_y}) \tag{8}$$

$$\frac{1}{R_x} = \frac{1}{R_{1x}} + \frac{1}{Rx} \tag{9}$$

$$\frac{1}{R_y} = \frac{1}{R_{1y}} + \frac{1}{R_{2y}} \tag{10}$$

According to the Hertzian theory it is assumed that the point contact turns into an ellipse when a normal load is applied to the two contacting bodies. An ellipcity parameter k_e occurs:

$$k_e = \frac{a_e}{b_e} \tag{11}$$

as a_e and b_e are semi-minor and semi-major axes of this ellipse geometry [13]. k_e can also be defined as as a function of curvature difference R_d, and the elliptic integrals of the first ξ and second ζ kind as described in [12]:

$$k_e = \left[\frac{2\xi - \zeta(1+R_d)}{\zeta(1-R_d)} \right]^{1/2} \tag{12}$$

where

$$\xi = \int_0^{\pi/2} \left[1 - (1 - \frac{1}{k_e^2}) \sin^2 \varphi \right]^{-1/2} d\varphi \tag{13}$$

$$\zeta = \int_0^{\pi/2} \left[1 - (1 - \frac{1}{k_e^2}) \sin^2 \varphi \right]^{-1/2} d\varphi \tag{14}$$

Hamrock et al. [13] used one point iteration and curve fitting techniques and obtained the approximation formulae, given in the appendix, for the integrals in Eqs(12-14). Then the contact stiffness coefficient for the elliptical contact assumption can be calculated as:

$$K_c = \pi \bar{k}_e A E' \sqrt{\frac{R\bar{\xi}}{4.5\bar{\zeta}^3}} \tag{15}$$

where the effective modulus of elasticity, E' is defined as:

$$\frac{1}{E'} = \frac{1}{2}\left(\frac{1-\upsilon_1^2}{E_1} + \frac{1-\upsilon_2^2}{E_2} \right) \tag{16}$$

where E is the modulus of elasticity, υ is the Poisson's ratio and the subscripts refer to solids 1 and 2. In the case of ball bearing, both of the solids have the same elasticity properties [8].

Damping at ball bearings is generally caused by lubrication. Also material damping is a factor that affects the total damping at contact region. In this current paper, a constant damping value, based on the experimental data, is used due to the relatively small damping in the bearing.

2.2 Bearing Defect Frequencies

Due to the geometric restrictions in rolling bearings, different components have different rotational speeds and velocities. This is the main reason for excitations at different frequencies which are called "defect frequencies". The vibration amplitudes at these frequencies are usually significantly higher than those at other frequencies when the component is defected. Also a ball bearing with no damage generates vibrations at a shaft speed dependent frequency which is called Ball Passing Frequency (BPF). BPF has the same value with outer ring defect frequency. If n_i and n_o are the rotational speeds of inner and outer rings (in rpm) , d indicates ball diameter and α indicates contact angle, N_b is the number of balls, then the so called defect frequencies are given as follows:

Fundamental Train Frequency (Cage speed):

$$FTF = \frac{1}{2}[n_i(1-\frac{d\cos\alpha}{d_m}) + n_0(1+\frac{d\cos\alpha}{d_m})] \tag{17}$$

Ball pass frequency outer ring:

$$BPFO = \frac{N_b}{120}[(n_i - n_0)(1-\frac{d\cos\alpha}{d_m})] \tag{18}$$

Ball pass frequency inner ring:

$$BPFI = \frac{N_b}{120}[(n_i - n_0)(1+\frac{d\cos\alpha}{d_m})] \tag{19}$$

Ball spinning frequency:

$$BSF = \frac{N_b}{120}[\frac{d_m}{d}(n_i - n_0)(1-(\frac{d\cos\alpha}{d_m})^2] \tag{20}$$

3 MBS MODEL OF A ROTOR-BALL BEARING SYSTEM

3.1 Modeling the ball bearing

In this study, a deep-groove ball bearing with a particular geometry is chosen to be modeled. The assumptions made during this process are listed below:

- The inner and outer rings and rolling elements are rigid.
- The contact stiffness between the rings and balls are determined due to the Hertzian Theory as described in the section 2.
- The cage is modeled with rigid connectors.
- The balls are positioned equi-pitched around the inner ring and there is no interaction between them.
- The damping caused by EHD contacts is assumed to be negligible.

The rigidity assumption of the ball bearing components can limit the observation of high frequency vibrations. On the other hand, a flexibility assumption of these components leads to a severe increase in CPU requirements.

After the 3D models of the ball bearing components (rings and balls) are imported to the ADAMS environment, the paths on which the components get into contact are defined. As shown in Figure 2, these paths are defined as curves. The balls and the races get into contact on these paths. In ADAMS software, this kind of contacts can be defined either as solid to solid or curve to curve. Although solid to solid contact option is attractive, this choice will increase the CPU times very significantly and, when the structure becomes more complex after the rotor part is added, the CPU requirements can easily exceed acceptable limit. Furthermore it is observed that, the model with curve to curve assumption can yield satisfactory results.

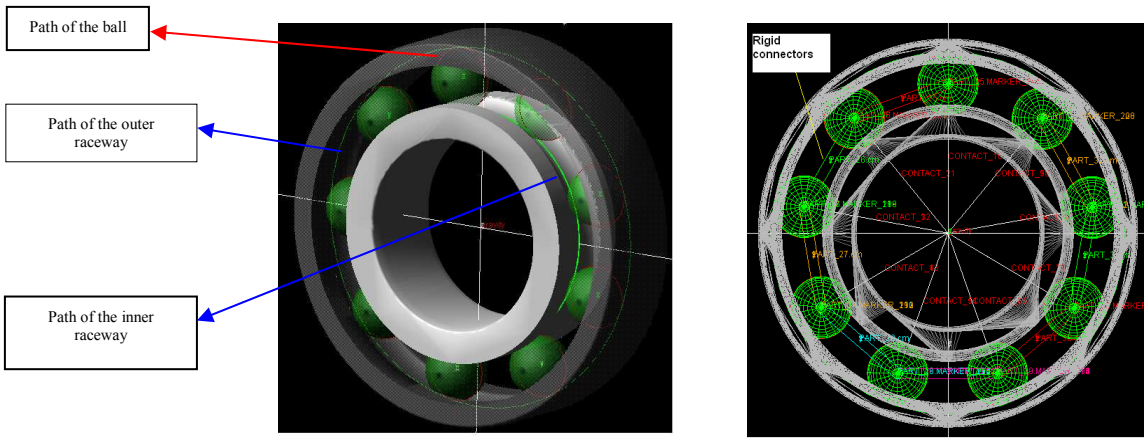

Figure 2. a) The ball bearing model and the defined paths **b)** The ADAMS model of the ball bearing

The balls of the bearing are connected to each other using rigid connectors. These rigid connectors represent the cage of the ball bearing. This contact type also enables modeling the diametral clearance and contact angles. By adjusting the size of the path a gap between a ball and ring can be created, representing the diametral clearance.

After the paths and contacts are defined, the kinematical relationships between the parts have to be specified. For the model of the ball bearing itself, the outer ring is supposed to be fixed to the ground. After the housings are assembled this constrain is changed. Balls, outer ring and inner ring are constrained to be in the same plane by using planar joints. Inner ring is fastened on balls. The final state of the ball bearing model is shown in Figure 2b.

3.2 Modeling the rotor and the housings

After the ball bearing model is created, the rotor part is built as a shaft and a disc at one the end of the shaft. As far as the shaft is concerned, two cases are considered. In the first case, it is assumed that the shaft is rigid. In the second case, however, a Finite Element (FE) model of the shaft is developed in order to include its flexibility in the model. Flexible shaft model consists of three dimensional beam elements. Disc part at the free end of the shaft is assumed to be rigid. Both of the models are shown in Figure 3.

The contact definition between the shaft and the inner ring of the ball bearing is also an important criteria. Although very limited, deep groove ball bearings have some rotational freedoms around radial axes. This freedom can have significant influence on the natural frequencies and dynamic behaviour of the system. In the proposed model, these freedoms are defined by using a bushing element with rotational stiffness between the inner rings and the shaft.

Housings are modelled using Frequency-Dependent (FD) damper utility in Msc. ADAMS software. Stiffness and damping coefficients of the housings obtained from experimental modal analysis are embedded in the model via these FD damper elements. It is assumed that the housing have stiffness and damping in radial directions whereas ball bearings are assumed to be fixed on the axial direction. After the model is validated for the non-rotating case via modal analysis, the model is run-up to 1000 rpm in 20 seconds and acceleration data are recorded on the bearings in vertical direction. Analyses are performed for various levels of unbalance, and defect conditions. Finally, FFT and STFT (short-time Fourier transform) are processed and Campbell diagrams are obtained using simulated data.

In what follows, an experimental procedure is described and then the numerical and experimental results are presented and compared.

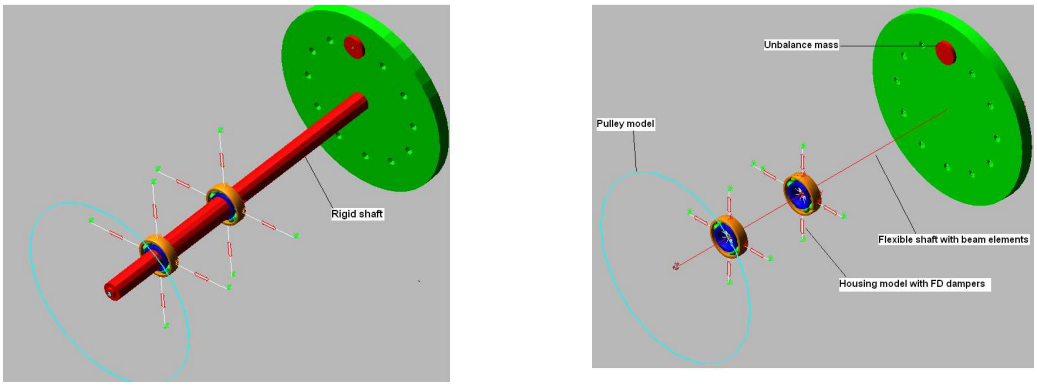

Figure 3. a) MBS model of the assembly with rigid shaft **b)** Model with flexible shaft

4 EXPERIMENTAL PROCEDURE

The test rig designed for the validation process is shown in Fig. 4. A heavy rigid block is used as a bench and it is isolated from the ground using soft supports. A separate AC motor is used for driving the rotor. A pulley-belt mechanism is used for power transmission from motor to the rotor. The test rig is designed such that the ball bearing, shaft and disc components can be disassembled easily. This allowed replacing individual components quickly and made it possible to experiment with various components with different characteristics. The disc had some holes which allowed mounting mass for creating unbalance. Modal characteristics of the system are identified using measured Frequency Response Function (FRF). For this purpose, an impact hammer is used as an exciter and an accelerometer was used for response measurement. Dynamic characteristics of the system under different rotational speeds are observed with Order Tracking analyses that are performed using the data recorded during the run-up period. A calibrated taco probe on the AC motor is used for revolution data. Vibration data are collected using accelerometers attached to the housings. Repeatability of the measurements and the calibration of the system are checked before recording data during both static and dynamic measurements.

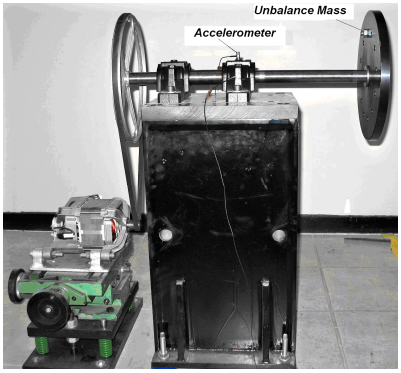

Figure 4. The Test Rig

5 RESULTS AND DISCUSSION

For the static (non-rotating) case, natural frequencies are determined using the numerical model developed. Natural frequencies of the system are also determined experimentally using the measured data. Results ate listed in Table 1. It is seen that the natural frequencies for the bending modes of the rotor-bearing system in vertical and horizontal directions are somewhat different. It is obvious that the system is not symmetric in vertical and horizontal directions. This asymmetry is a result of the housings' and belt's stiffnesses being different in horizontal and vertical directions. Damping values are also assumed to be different in horizontal and vertical directions.

The numerical model has some parameters for the housings' and belt's stiffnesses in vertical and horizontal directions. These parameters are tuned in the light of the experimental data so as to produce the predicted natural frequencies as close as to the experimental values. It is seen in Table 1 that the corrected numerical model can

yield natural frequencies quite close to the measured values. As one might expect, the numerical results presented in Table 1 are obtained when the flexible shaft model is used in the numerical model.

Mode type	Numerical (Hz)	Experimental (Hz)
Horizontal Bending	28.36	27.21
Vertical Bending	30.25	31.35
Torsional	45.82	44.72
Horizontal Bending	169.27	167.73
Vertical Bending	174.65	174.48

Table 1. Comparison of Natural Frequencies

For the dynamic case, a run-up procedure up to 1000 RPM is simulated numerically and the same situation is created in reality using the test rig. . A 66 g unbalance mass is attached to the disc in order to create rotating unbalance force. The Campbell diagrams based on numerical and experimental data are shown in Figures 5, 6, 7. As expected, the model with rigid shaft assumption is not capable of representing modes associated with shaft bending (Figure 5). The mode identified as the "rocking mode" in Fig.5 for the rigid shaft case is the one which can be described as the vertical motion of the shaft and the inner ring inside the outer ring. This frequency is strongly related with contact stiffness and clearance. Although the vibrations at the harmonics of running speed are not visible in the rigid shaft case, BPF and its harmonics can be clearly seen.

The Campbell diagram obtained from the numerical model based on flexible shaft is shown in Figure 6 and the Campbell diagram based on experimental data are shown in Figure . In both Campbell diagrams the 1^{st} harmonic has very high amplitudes as a result of unbalance. Also in both figures Outer Ring Ball Passing Frequency (BPFO) with the sidebands are visible. It should be noted that the experimental results indicate vibrations at the 11^{th} harmonic of the running speed. This corresponds to the speed of electric motor which drives the test rig. The vibrations transmitted from the motor are not included in the numerical model; hence it is not visible in Fig.6.

The natural frequencies of the system corresponding to the bending modes split from each other while the running speed increases. This is due to the gyroscopic effects which are quite significant for overhung rotors [15]. In both experimental (Figure 7) and numerical (Figure 6) Campbell diagrams these gyroscopic effects are visible. While modelling the rotor-bearing system in Msc. ADAMS, the gyroscopic effects of the disc is included in the model [16]. It can be seen from both Figures 6 and 7 that the frequency split for 2^{nd} bending modes is more significant than the 1^{st} ones.

A case study with a ball-bearing which has a defect on the outer ring and a 66 g unbalance mass on the disc is also carried out, both numerically and experimentally. The localized defect is modelled with a small bump on the outer path. The numerical and experimental frequency spectrums at 1180 RPM are shown in Figure . It can be argued that the BPFO and its' side bands are visible in both cases. Also, the predicted and the experimental amplitude levels are quite close to each other. However, the level of correlation between the predicted and the measured spectrums decreases at higher frequencies.

6. CONCLUDING REMARKS

A dynamic model of an overhung rotor-bearing system is built with multibody system approach and it is validated using experimental results. The elements of the ball bearing are assumed to be rigid, but the stiffness properties related to contact characteristics are included in the model. For non rotating case, the first few natural frequencies corresponding to bending and torsion modes are predicted with acceptable accuracy. The model is capable of representing the modal characteristics and the change of these characteristic due to gyroscopic effects.

Critical speeds, bearing defect frequencies and the response of the system under certain unbalance conditions are studied. It is clear that the flexibility of the shaft must be included in the model in order to predict the important features of the rotor-bearing systems.

The rings of the bearing are assumed to be rigid in this study. The flexibility of the rings needs to be included if the vibrations at higher frequencies due to the modal characteristics of rings are of interest. Also, the housing can also be modelled using Finite Element approach for improved accuracy.

.

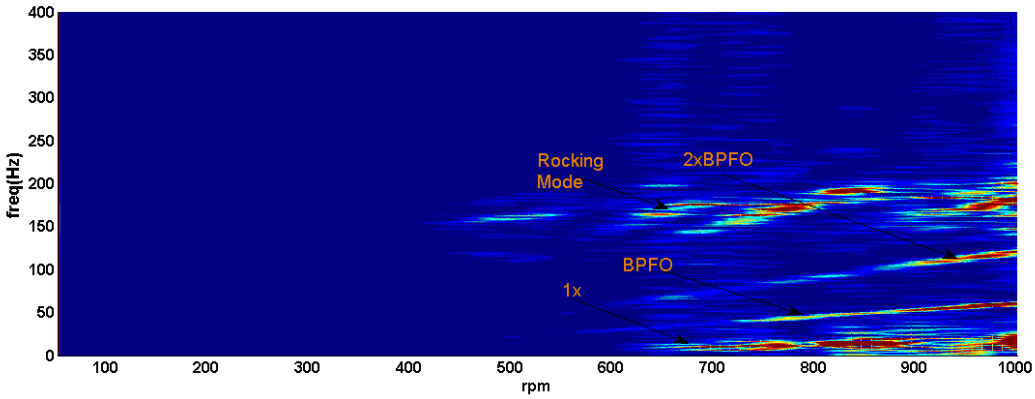

Figure 5. Campbell Diagram obtained from the ADAMS model with rigid shaft

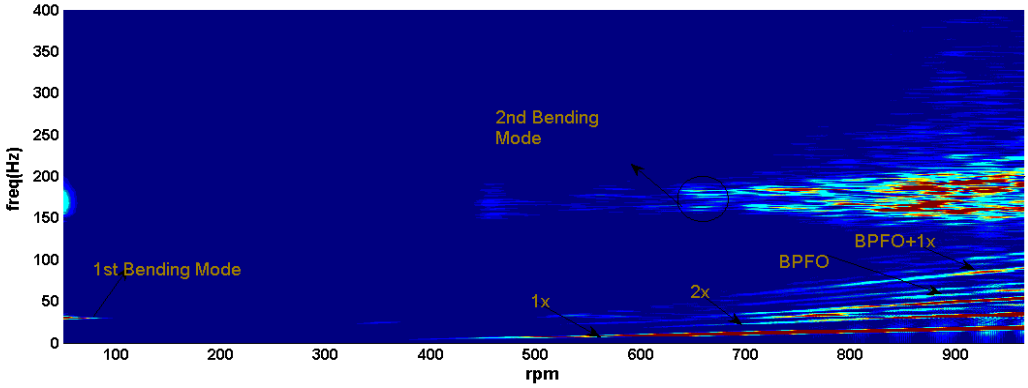

Figure 6. Campbell Diagram obtained form the ADAMS model with flexible shaft

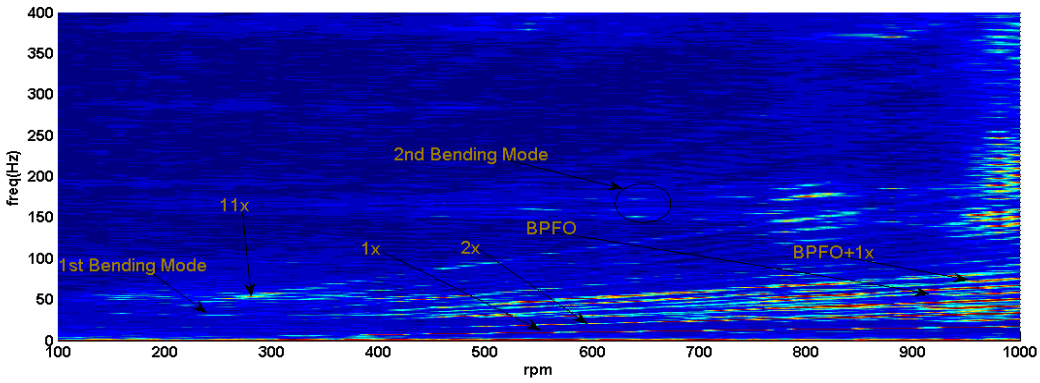

Figure 7. Campbell Diagram obtained from the experiments

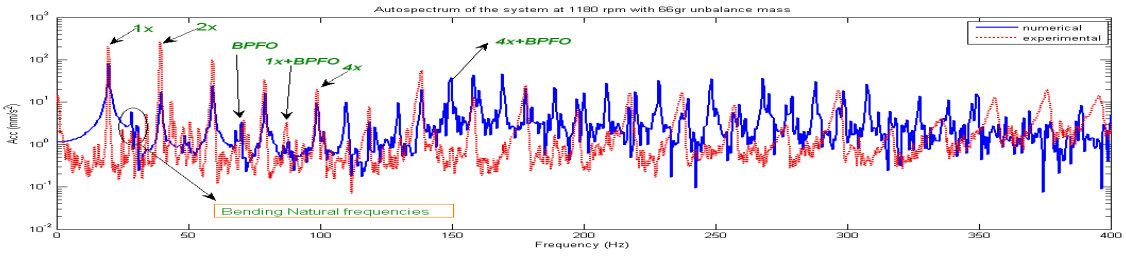

Figure 8. Amplitude spectrum of the system with a defected ball bearing

REFERENCES

[1] **T**ANDON, N AND **C**HOUDRY, A. An analytical model for the prediction of the vibration response of rolling elements due to localized defect. *Journal of sound and vibration 205*, 3(1997), 275-292.

[2] **T**ANDON, N AND **C**HOUDRY, A. A theoretical model to predict vibration response of rolling elements due to distributed defects under radial load. *Journal of vibration and acoustics*, 120, (1998), 214-220.

[3] TIWARI, M. AND **G**UPTA, K**.** Effect of radial internal clearance of a ball bearing on the dynamics of a balanced horizontal rotor. *Journal of sound and vibration*, *238*, 5 (2000), 723-756.

[4] TAMURA, H. AND **T**SUDA, Y. On the static running accuracy of ball bearings. *Bulletin of the JSME, 28*, (1985), 1240-1246.

[5] TIWARI, M. AND **G**UPTA, K**.** Dynamic response of an unbalanced rotor supported on ball bearings. *Journal of sound and vibration*, *238*, 5 (2000), 757-779.

[6] AKTURK, N., **U**NEEB, M. AND **G**OHAR, R. The effects of number of balls and preload on vibrations associated with ball bearings. *Journal of Tribology, 1119,* (1997), 747-753.

[7] WENSING, J. A. On the dynamics of ball bearings. Phd Thesis (1998), University of Twente, the Netherlands.

[8] SOPANEN, J. AND **M**IKKOLA, A. Dynamic model of a deep groove ball bearing including localized and distributed defects, part 1: theory. *Journal of Multi-body Dynamics*, *217*, 4 (2003), 201-211.

[9] SOPANEN, J. AND **M**IKKOLA, A. Dynamic model of a deep groove ball bearing including localized and distributed defects, part 1: implementation and results. *Journal of Multi-body Dynamics*, *217*, 4 (2003),211-221.

[10] ROYSTON, T. J. AND **B**ASDOGAN, I. Vibration transmission through self-aligning (spherical) rolling element bearings: theory and experiment. *Journal of Sound and Vibration, 215*, 5 (1998), 997-1014.

[11] HARRIS, T. A**.** *Rolling Bearing Analysis,* Wiley & Sons, New York, USA, 1993.

[12] HAMROCK, B. J. *Fundamentals of Fluid Film Interaction,* Mc-Graw Hill, New York, 1994.

[13] HAMROCK, B. J. AND **D**AWSON, D**.** Isothermal elastohydrodynamic lubrication of point contacts, part 1: theoretical formulation, *Journal of Lubrication Technology, 98,* (1976) ,223-229.

[14] KRAMER, E**.** *Dynamics of Rotors and Foundations*, Springer-Verlag., New York, 1993.

[15] GOODWIN, J. M. "*Dynamics of Rotor-Bearing Systems*, Unwin Hyman Ltd., London, 1989.

[16] ORTIZ J. L**.** AND **B**IR, G. S. Verification of new Msc.ADAMS linearization capability for wind turbine. In *Proceedings of 44th AIAA Aerospace Sciences Meeting and Exhibit* (Reno, Nevada, USA, 2006)

APPENDIX

Hamrock et al. e and [13] used one point iteration and curve fitting techniques and obtained the approximation formulae given below for the determination of elliptic integrals:

$$\bar{k}_e = 1.0339\left(\frac{R_y}{R_x}\right)^{0.6360} \qquad \bar{\xi} = 1.0003 + 0.5968\frac{R_x}{R_y} \qquad \bar{\zeta} = 1.5277 + 0.6023\ln\left(\frac{R_y}{R_x}\right)$$